

A low aspect ratio electrothermal gun for metal plasma vapor discharge and ceramic nanopowder production

Kyoungjin Kim^{1,*} and Dennis R. Peterson²

¹*School of Mechanical Engineering, Kumoh National Institute of Technology, Geongbuk 730-701, Korea*

²*Peterson Science and Technology, Malvern, PA 19355, U.S.A.*

(Manuscript Received November 16, 2007; Revised April 6, 2008; Accepted April 16, 2008)

Abstract

Traditionally, the electrothermal gun design has the bore of a large aspect ratio; however, a low aspect ratio design with a shorter bore length has been employed for efficient production of metal plasma vapors and synthesis of nanomaterials. In a comparison of the arc resistance-current relationship, a low aspect ratio design is found to exhibit distinctively different characteristics compared to a high aspect ratio design, and this trend is explained by the scaling law of plasma properties including theory of plasma electrical conductivity. A one-dimensional isothermal model has been applied to the present experiments to confirm the scaling laws, and it was found that the present modification of the electrothermal gun is able to produce fully ionized metal plasma vapor, while the plasma vapor produced in a conventional design is partially ionized. Also, by reacting metal plasma vapors with the controlled gases in the reaction chamber, nanoscale materials such as aluminum oxide, aluminum nitride, and titanium oxide were synthesized successfully.

Keywords: Electrothermal gun; Metal plasma vapors; Plasma vapor discharge; Nanomaterial synthesis

1. Introduction

Electrothermal guns or electrothermal-chemical guns were originally developed to improve the acceleration of projectiles by using high-pressure and high-velocity plasma jet as an alternative to the conventional propellant igniter [1-6]. Traditionally, the electrodes use erosion-resistant metals such as tungsten alloy, and the aspect ratio of bore length to diameter is large and the order of ten. These devices rely on the erosion of the bore wall, which is typically made of organic materials such as polyethylene or polycarbonate, by high-magnitude current pulses and subsequent intense Joule heating. In this article, a modification of the electrothermal gun is discussed for the generation of various kinds of metal and carbon plasma vapors, which can be used in the synthesis of

novel nanophase materials and nanocoating techniques on the substrates. The process employs electrode erosion to vaporize one or both of the electrodes, and the eroded metal vapor is subsequently ionized to form a dense plasma through which a high current discharge is sustained. The vapor plasma then exits the open end of the bore to create a high-velocity, high-temperature, high-pressure, and highly ionized external plasma jet in the controlled background gas in the reaction chamber.

Table 1 shows electrothermal gun configurations of conventional and present designs. The aspect ratio of the present design is much smaller ($L/D = 2$) compared to the case of conventional types ($L/D \approx 10$). As the bore length becomes shorter and the distance between the electrodes shortens, the present design of the electrothermal gun is rather similar to the electric arcs between the electrodes rather than traditional electrothermal gun concept. However, in usual electric arc devices, the evaporation of the electrode is normally undesirable and the erosion is on the order

*Corresponding author. Tel.: +82 54 478 7890, Fax.: +82 54 478 7319
E-mail address: kimkj@kumoh.ac.kr
DOI 10.1007/s12206-008-0414-9

of 1–10 mg.

Also, this study seeks an efficient method of synthesizing nanopowders by utilizing metal plasma vapors, which discharge into the reaction chamber and react with the controlled gases to produce sub-100 nm nanosized metal oxide and nitride particles.

2. Experiments

Fig. 1 shows a schematic diagram of the electrothermal gun and the experimental setup. A pulse-forming network (PFN) consists of the capacitor bank (C), inductors (L), resistors (R), and the ignition switch, and it provides high-current pulsed power to an electrothermal gun. Both the capacitors and the inductors can be varied to apply a wide variety of current, energy, voltage, and pulse duration time. The maximum voltage from the capacitor bank is 11 kV, while the maximum output current is 500 kA. The maximum energy stored in the capacitor bank is approximately 1.2 MJ.

The bore of the electrothermal gun is 6.65 mm in diameter and 13.5 mm in length ($L/D = 2$) and made of erosion-resistant aluminum oxide. Additionally, the bore length of 40 mm ($L/D = 6$) has been tested with the same bore diameter for comparative pur-

poses. The electrodes are made of aluminum, titanium, and graphite to produce metal and carbon plasma vapors. When the ignition switch (S1) is closed, current discharge is then initiated and the electrodes are explosively vaporized. The plasma column inside the bore is subjected to intense Joule heating. The resulting high-pressure plasma expands rapidly from an open end of the bore into the chamber in the form of a highly underexpanded supersonic jet and experiences a high rate of quenching.

Fig. 2 shows the measured temporal traces of breech voltage, arc current, and energy deposition for producing aluminum plasma vapor for the condition of initial capacitor charging voltage of 5.1 kV and energy deposition of 96 kJ. The pulse duration was approximately 1.1 ms, while the maximum current was 99 kA at 0.46 ms after the electrothermal gun was triggered. Note that the voltage spike at the initiation of energy release is due to the explosion of aluminum fuse wire initially installed between the electrodes for establishing the current path in the bore. Fig. 3 shows the eroded aluminum cathode after a single gun firing, and the mass loss of the cathode is 0.13 g after the electrothermal gun operation with the energy deposition of 96 kJ and time duration of 1.1 ms.

After metal plasma vapors were discharged and reacted with the controlled background gas in the reaction chamber, the synthesized nanopowders were allowed to settle down on the collection plate in the reaction chamber. The material contents in the collected sample were tested by the X-ray diffractometer (XRD) to identify the crystalline structure of the syn-

Table 1. Dimensions and operating conditions of electrothermal guns.

	D (mm)	L (mm)	L/D	Edep (kJ)	Max. I (kA)
present	6.7	13.5	2	-	-
Powell and Zielinski [5]	7.8	60.9	7.8	47	58.7
Kim et al. [3]	3.1	30	9.7	3.1	4.6
Loeb and Kaplan [7]	4	50	12.5	N/A	30

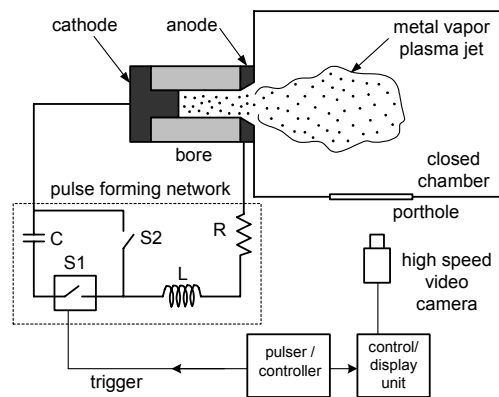


Fig. 1. Schematic diagram of electrothermal gun experimental setup.

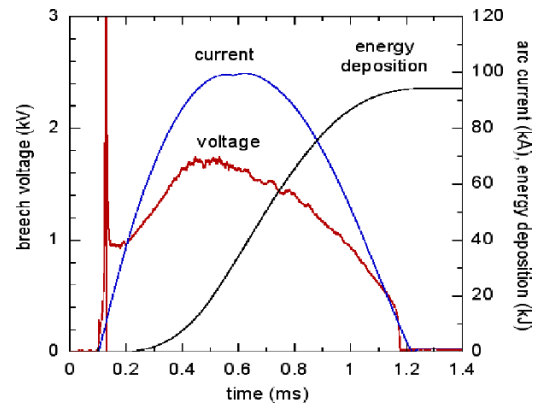


Fig. 2. Measured temporal traces of breech voltage, arc current, and energy deposition for aluminum plasma vapor (initial capacitor charging voltage of 5.1 kV and energy deposition of 96 kJ).



Fig. 3. Eroded aluminum cathode after electrothermal gun operation with energy deposition of 96 kJ.

thesized material. Particle morphology was investigated by using a Hitachi S-4500 field emission scanning electron microscope (SEM) and JEOL 200CX transmission electron microscope (TEM). Also, the Brunner-Emmett-Teller (BET) method was used to measure the specific surface area (SSA) of the collected powder samples.

3. Results and discussion

3.1 Scaling law analysis of arc conductance

A relationship between the arc conductance and the corresponding arc current in the experiments of gun firing with carbon, titanium, and aluminum cathode are compiled in Fig. 4, along with the measured data from three previous electrothermal gun tests [3, 5, 7]. It is found that the data from conventional electrothermal gun fall into the trend of $1/R \sim I^{0.72}$ despite the fact that they possess much different bore dimensions and the degree of energy deposition. This trend could be verified from the present measurements of aluminum vapor shot with the bore length of 40 mm ($L/D = 6$), as shown in Fig. 4 and the best fit is found to be

$$1/R = 1.55I^{0.72} \tag{1}$$

In contrast, from the trend found in the gun operations with much shorter bore of $L/D = 2$, the power curve fit is found to be

$$1/R = 5.44I^{0.54} \tag{2}$$

which is distinctively different from the electrothermal gun with a larger aspect ratio. This could be ex-

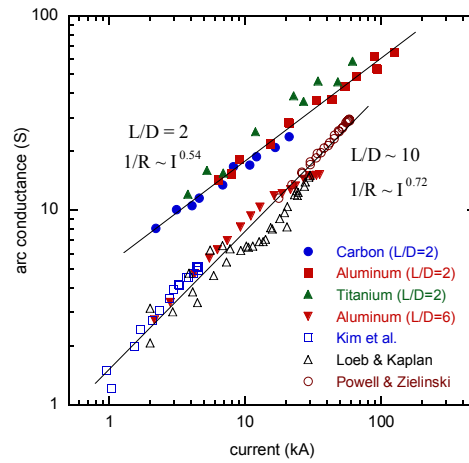


Fig. 4. Measured arc conductance as a function of arc current. Filled symbols represent present experiments and open symbols are from conventional electrothermal gun measurements [3, 5, 7].

plained by the following simple scaling laws utilizing the theory of plasma electrical conductivity [8] and the energy conservation principle of Joule heating in the capillary bore. Electrical conductivity of fully or partially ionized gases is given as

$$\frac{1}{\sigma} = \frac{1}{\sigma_{ei}} + \frac{1}{\sigma_{en}} = \frac{m_e(\bar{v}_{ei} + \bar{v}_{en})}{n_e e^2} \tag{3}$$

For fully ionized gases, the Spitzer formula [8] gives electron-ion collision frequency, \bar{v}_{ei} , as

$$\bar{v}_{ei} = \frac{38Z_{eff}n_e e^2}{\gamma_e m_e T^{3/2}} \ln(1 + 1.4\Lambda_m^2)^{1/2} \tag{4}$$

after considering the correction due to nonideal dense plasma according to Liebermann and Zollweg [9]. The electron-neutral collision frequency \bar{v}_{en} is expressed as

$$\bar{v}_{en} = n_0 \bar{Q}_{e0} \sqrt{\frac{8kT}{\pi m_e}} \tag{5}$$

Total electrical conductivity can be expressed in another form such as $\sigma = \beta \sigma_a$, where $\beta = (1 + \bar{v}_{en}/\bar{v}_{ei})^{-1}$ becomes a correction factor for the presence of neutral species to the traditional Spitzer formula of fully ionized gases. Plasmas are expected to be in local thermodynamic equilibrium in a typical electrothermal gun operation. Therefore, the composition and the thermodynamic properties of the plasma can be determined from the local state of the plasma by solv-

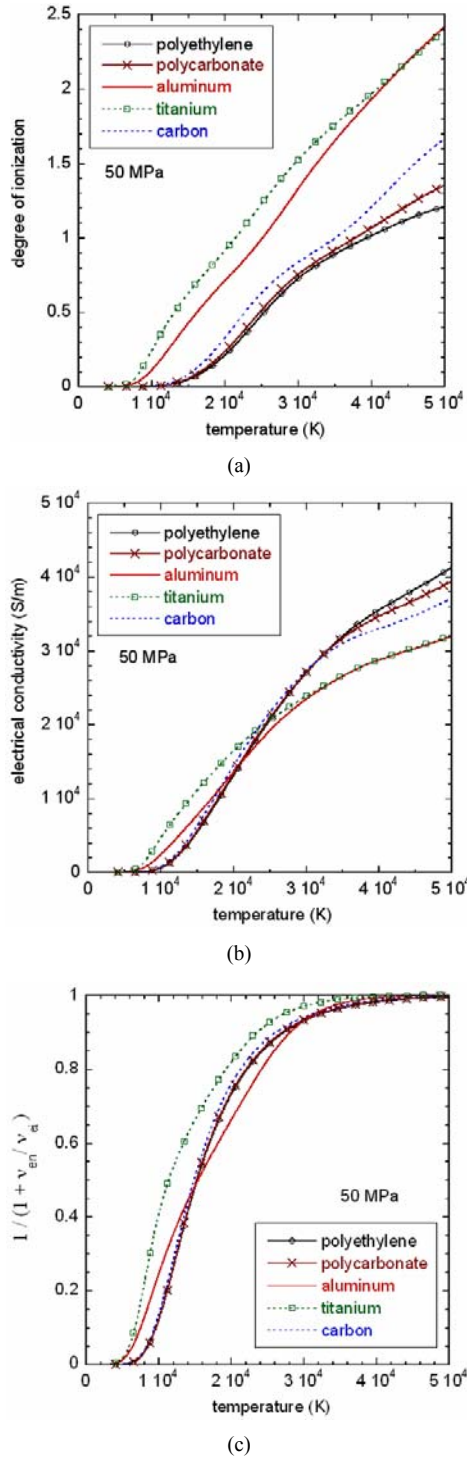


Fig. 5. Thermophysical properties of polyethylene, polycarbonate, aluminum, titanium, and carbon plasmas at 50 MPa. (a) degree of ionization; (b) electrical conductivity; (c) correction factor of electron-neutral species collision to electrical conductivity.

ing Saha equations with the consideration of lowering of ionization energy due to weak plasma nonideality. Figs. 5(a) and (b) show the calculated electrical conductivity and degree of ionization in a local thermodynamics equilibrium condition for the plasmas of carbon, titanium, aluminum, polycarbonate, and polyethylene materials at the pressure of 50 MPa, which is a typical condition in the electrothermal gun operations. Fig. 5(c) presents the correction factor to the neutral species which becomes constant at higher temperature or 40,000 K at 50 MPa.

In a capillary plasma discharge, we may assume that the Joule heating is proportional to the radiative heating from plasma column to the bore wall [5, 7]. Therefore, we have

$$\sigma_{sb} T^4 \sim \frac{J^2}{\sigma} \tag{6}$$

If the plasma vapor in the bore is fully ionized and the plasma bulk temperature is approximately at or above 40,000 K, we expect that the electron-neutral collisions become negligible ($\beta \approx 1$), as shown in Fig. 5(c), and the electrical conductivity is proportional to $T^{3/2}$. Thus, we find the relationship of $J^2 \sim \sigma T^4 \sim \sigma^{11/3}$ or $\sigma \sim J^{6/11}$ ignoring the Stefan-Boltzmann constant. Therefore, the arc conductance ($1/R \sim \sigma$) and arc current ($I \sim J$) relationship is given as

$$1/R \sim I^{6/11} \sim I^{0.55} \tag{7}$$

This result is consistent with the measured trend of arc conductance with arc current change in the present design of an electrothermal gun.

On the contrary, plasma vapors in traditional designs with a larger aspect ratio are only partially ionized. In a study by Kim [10], polycarbonate vapor does not reach full ionization and electron-neutral collisions are significant compared to electron-ion collisions. In those cases where plasma bulk temperature in the bore falls between 20,000~30,000 K, the correction factor β appears to be proportional to T , which results in the relationship of $\sigma \sim T^{5/2}$ for partially ionized gases. Therefore, similarly as in previous scaling law analysis, we find $J^2 \sim \sigma T^4 \sim \sigma^{13/5}$ or $\sigma \sim J^{10/13} \sim J^{0.77}$. Therefore, conductance of plasma in the bore is found to be

$$1/R \sim I^{10/13} \sim I^{0.77} \tag{8}$$

This is close to the power law of $I^{0.72}$ which is found in the measurements from traditional electrothermal guns. In summary, due to smaller bore aspect

ratio and ablation friendly electrode materials, the present design of the electrothermal gun produces fully ionized plasma vapor, while the traditional design produces partially ionized plasma.

3.2 Isothermal model of bore plasma

A simple quasi-steady isothermal model by Powell and Zielinski [5] was used to estimate the plasma conditions in the present experiments. Despite the simplicity of the model, isothermal approximation has been found to be reliable in predicting bore plasma properties in the electrothermal gun operations. By the energy conservation, as mentioned earlier, isothermal plasma temperature is given as

$$T = \left(\frac{J^2 D}{4\sigma\sigma_{sb}} \right)^{1/4} \tag{9}$$

and the mass flow rate is given as

$$\rho u = \dot{\rho}_b L + \dot{m}_c \tag{10}$$

where $\dot{\rho}_b$ represents the ablation mass influx of bore material into the bulk plasma.

$$\dot{\rho}_a = \frac{4\sigma_{sb} T^4 / D}{\varepsilon + P / \rho} \tag{11}$$

In this model, evaluation of ablation mass influx of cathode material, \dot{m}_c , is expected to be predominantly by thermal evaporation, and the prediction of evaporation rate was found to be problematic, since there is no simple method for a reliable prediction. One possibility would be the well-known Hertz-Knudsen formula; however, when that formula is used in the computations, the predicted erosion of aluminum cathode is found to be approximately five times higher than the measurement. This may be due to the formation of a melting layer on the electrode surface and mechanical erosion by shear flow in such an extreme condition of electrothermal gun operation. Therefore, in this study, the experimental data of measured cathode erosion has been supplied into this model and, for example, the eroded mass is 0.13 g for the aluminum cathode ($L/D = 2$ and 5.1 kV initial capacitor voltage). In order to close the problem, bore plasma flow is assumed to obey the ideal gas approximation and sonic condition due to the choking at the bore exit.

$$P = \frac{k}{m} (1 + \alpha) \rho T \quad \text{and} \quad c_s = \left(\gamma_{eff} (1 + \alpha) R_h T \right)^{1/2} \tag{12}$$

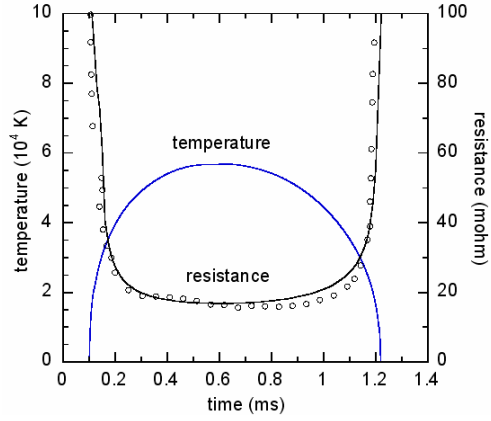
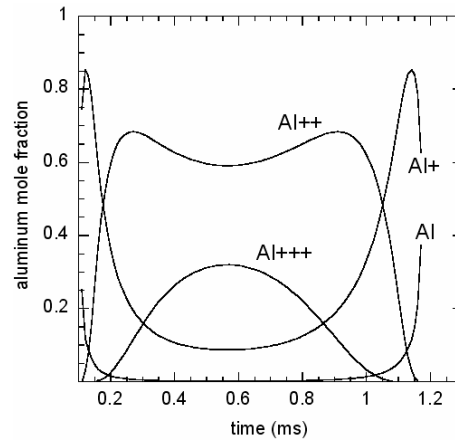
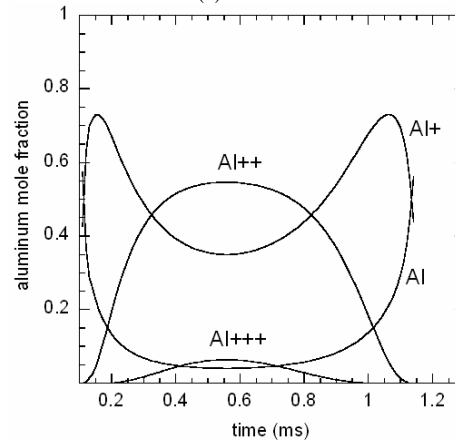


Fig. 6. Arc resistance and temperature of bore plasma from the isothermal plasma model (aluminum cathode, $L/D = 2$, and 5.1 kV initial capacitor voltage). Symbols represent the measured arc resistance.



(a) $L/D=2$



(b) $L/D=6$

Fig. 7. Calculated mole fraction of aluminum heavy species in the bore plasma from aluminum cathode erosion. (a) $L/D = 2$; (b) $L/D = 6$.

The above set of equations is coupled into the Saha equation for the calculation of thermodynamic and transport properties such as degree of ionization and electrical conductivity of plasma, and the numerical scheme requires iterations to obtain solutions for a given arc current and the bore geometry at each time step.

The predicted plasma temperature is shown in Fig. 6 and the maximum temperature is found to be 56,800 K, which is significantly higher than predicted plasma temperature of 20,000–30,000 K for conventional electrothermal gun operations [10]. Also, in Fig. 6, arc resistance, which is calculated based on plasma electrical conductivity, is compared to the measured data and the agreement is favorable. However, it should be noted that the arc resistance is much easier to predict than the other thermophysical properties of plasma. Fig. 7 shows the composition of heavy species in aluminum plasma with two aspect ratios of bore: $L/D = 2$ and 6. As expected, neutral species of aluminum is negligible and the degree of ionization level is relatively higher in a short aspect ratio design ($L/D = 2$). In the low aspect ratio design, a third level of aluminum ionization (Al^{+++}) is significant, while in a high aspect ratio design lower ionization levels (Al^+ and Al^{++}) are dominant. Combined with high plasma temperature at the bore exit implying a high expansion and quenching rate of plasma vapor, the low aspect ratio design may be more advantageous in various applications such as material synthesis via gas condensation to particles and chemical reaction with controlled background gas.

3.3 Nanoparticle synthesis by metal vapor condensation

Metal plasma vapor jets produced in the electrothermal gun were introduced into the reaction chamber filled with controlled background gas in order to synthesize the nanometric particles. Fig. 8 shows the XRD patterns of the produced nanopowders collected by the sedimentation in the reaction chamber. First, aluminum oxide (Al_2O_3) nanopowders were produced by the reacting of the aluminum plasma vapor with the background gas composed of 17 percent oxygen and 83 percent helium at atmospheric pressure. The crystalline structure of the sample is mostly γ -phase aluminum oxide and there is the very small amount of the α -phase content, as shown in Fig. 8(a). No other material such as aluminum was found in the sample. The formation of the metastable γ -phase over the

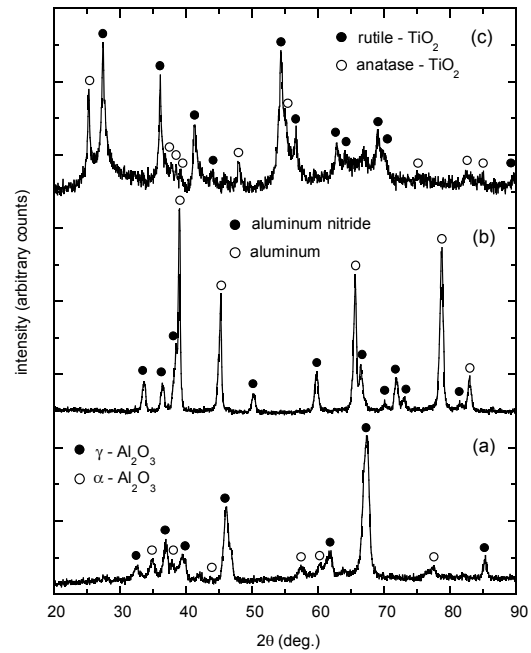


Fig. 8. XRD patterns of produced nanosized powders by metal vapor discharge in the reaction chamber. (a) aluminum cathode and 17 % O_2 / 83 % He; (b) aluminum cathode and 100 % N_2 ; (c) titanium cathode and 17 % O_2 / 83 % He.

thermodynamically stable α -phase is due to the very high quenching rate of the reacted metal vapor. Similar results are reported in several plasma-assisted nanomaterial production methods such as aluminum exploding wires [11] and DC plasma torch with the micron-sized aluminum powder oxidation [12]. In an attempt to synthesize aluminum nitride (AlN) nanopowders, the background gas of 100 percent nitrogen was tested with aluminum plasma vapor and, as shown in Fig. 8(b), the collected powder was found out to be a mixture of aluminum nitride in the crystalline form of wurtzite (hexagonal) and aluminum metal. In this case, aluminum vapor was not adequately reacted with nitrogen gas due to significantly higher dissociation energy in nitrogen gas than oxygen gas, and unreacted aluminum content including micron-sized particles was observed in the collected powder. In case of the titanium plasma vapor introduced into background gas of 17 percent oxygen and 83 percent helium, titanium oxide (TiO_2) nanopowder was synthesized and the crystalline structure of the sample was a mixture of metastable anatase and more thermodynamically stable rutile phases.

The morphology of the produced nanoparticles was also investigated by using SEM and TEM techniques.

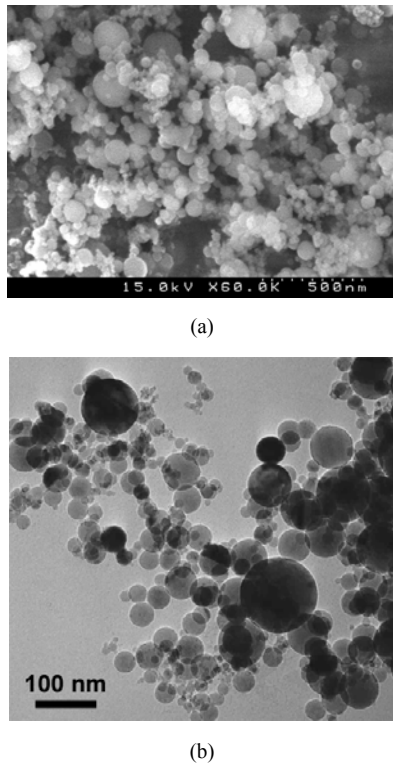


Fig. 9. SEM (a) and TEM (b) micrographs of produced aluminum oxide nanoparticles.

Figs. 9(a) and (b), which have micrographs of the collected aluminum oxide sample, show the fine aluminum oxide particles of the spherical shape with the diameter ranging mostly between 10 and 100 nm. Based on those micrographs, the particle size distribution of the aluminum oxide nanopowder was established, as shown in Fig. 10. As expected, the trend shows a typical lognormal distribution, and 90 percent of the total particles are distributed in the range below the diameter of 80 nm. From the statistical analysis, the geometric mean diameter (d_g) is found to be 40.3 nm and the geometric standard deviation (σ_g) is 1.60. Thus, the average particle diameter based on the surface area was found to be 50 nm. Meanwhile, the BET measurement showed a specific surface area (S) of approximately $30 \text{ m}^2/\text{g}$. By assuming spherical particles, the average particle diameter can be estimated such as $d = 6/\rho S$ where ρ is the density of the aluminum oxide ($3.97 \text{ g}/\text{cm}^3$). The estimated particle diameter is 50.4 nm, which is very consistent with the average diameter based on the SEM/TEM investigations. In addition, TEM micrograph of synthesize sized titanium oxide nanopowder is shown in Fig.

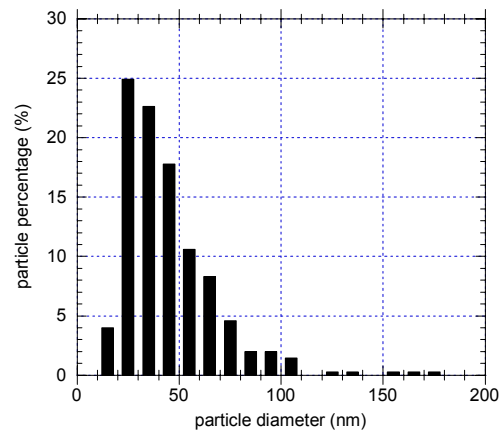


Fig. 10. Particle size distribution of produced aluminum oxide nanoparticles.

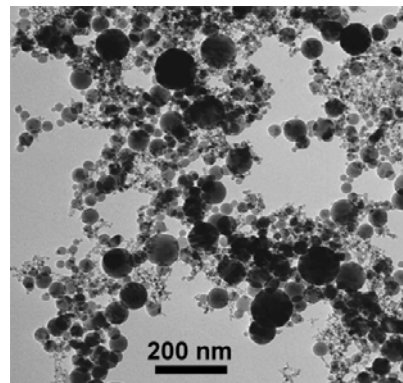


Fig. 11. TEM micrograph of produced titanium oxide nanoparticles.

11. Note that in carbon plasma discharge using graphite cathode, eroded mass was approximately 10 mg, which led to the difficulty of powder collection. Also, collected sample was found to be mostly amorphous and the present approach failed to produce crystalline structure of any carbon form, thereby requiring further study.

4. Conclusions

In this article, an electrothermal gun with a shorter bore length has been tested for the purpose of producing metal vapors by eroding metal cathodes with high current pulsed power. The arc resistance-current relationship is found to be different in a shorter aspect ratio design and a larger aspect ratio design, and this was successfully explained by the scaling laws using

electrical conductivity theory and the energy conservation principle. A longer bore in the present experiments is also tested to verify those findings.

With a quasi-steady isothermal model of plasma flow calculations, the plasma temperature in the present configuration was found to be extremely high above 50,000 K and the predicted arc resistance was in good agreement with the measurements. Also, a shorter bore length design was found to be more efficient in producing fully ionized metal vapor discharges with significant mole fraction of third ionization level ion species, while the traditional design with a longer bore produced partially ionized plasma vapors.

By introducing metal plasma vapors into the controlled background gas with extremely high expansion and quenching rate, we successfully synthesized various kinds of sub-100 nm nanosized powders such as aluminum oxide, aluminum nitride, and titanium oxide, which crystalline contents were verified by XRD and SEM/TEM techniques.

Nomenclature

c_s	: Speed of sound [m/s]
D	: Bore diameter [m]
e	: Electron charge [C]
I	: Current [A]
J	: Current density [A/m ²]
k	: Boltzmann constant [J/K]
L	: Bore length [m]
\bar{m}	: Average particle mass of heavy species [kg]
\dot{m}_c	: Ablation mass flux of cathode [kg/m ² · s]
m_e	: Electron mass [kg]
n_0	: Particle number density of neutral species [m ⁻³]
n_e	: Electron number density [m ⁻³]
P	: Pressure [Pa]
\bar{Q}_{eo}	: Electron-neutral momentum transfer cross section [m ²]
R	: Arc resistance [Ω]
R_h	: Average gas constant of heavy species [J/kg·K]
T	: Temperature [K]
u	: Axial velocity [m/s]
Z_{eff}	: Effective charge on a plasma ion

Greek Symbols

α	: Degree of ionization
----------	------------------------

β	: Correction factor to Spitzer formula
γ_e	: Correction factor for electron-electron scattering
γ_{eff}	: Effective specific heat ratio
ε	: Specific total energy [J/kg]
Λ_m	: Modified plasma parameter
ρ	: Total plasma mass density [kg/m ³]
$\dot{\rho}_a$: Mass ablation density rate [kg/m ³ ·s]
σ	: Plasma electrical conductivity [S/m]
σ_{sb}	: Stefan-Boltzmann constant [W/m ² ·K ⁴]
$\bar{\nu}_{ei}$: Electron-ion collision frequency [s ⁻¹]
$\bar{\nu}_{en}$: Electron-neutral collision frequency [s ⁻¹]

References

- [1] K. J. White, G. L. Katulka, T. Khong and K. Nekula, Plasma characterization for electrothermal-chemical gun, ARL-TR-1491, U. S. Army Research Laboratory (1997).
- [2] J. M. Kohel, L. K. Su, N. T. Clemens and P. L. Varghese, Emission spectroscopic measurements and analysis of a pulsed plasma jet, *IEEE Transactions on Magnetics*, 35 (1) (1999) 201-206.
- [3] J. U. Kim, N. T. Clemens and P. L. Varghese, Experimental study of an underexpanded pulsed plasma-jet, AIAA Paper-99-0452 (1999).
- [4] R. B. Mohanti and J. G. Gilligan, Time-dependent simulation of the plasma discharge in an electrothermal launcher, *IEEE Transactions on Magnetics*, 29 (1) (1993) 585-590.
- [5] J. D. Powell and A. E. Zielinski, Theory and experiment for an ablating-capillary discharge and applications to electrothermal-chemical guns, BRL-TR-3355 (1992).
- [6] M. J. Taylor, Measurement of the properties of plasma from ETC capillary plasma generators, *IEEE Transactions on Magnetics*, 37 (1) (2001) 194-198.
- [7] A. Loeb and Z. Kaplan, A theoretical model for the physical process in the confined high pressure discharges of electrothermal launchers, *IEEE Transactions on Magnetics*, 25 (1) (1989) 342-346.
- [8] L. Spitzer, *Physics of Fully Ionized Gases*, Interscience, New York (1956).
- [9] R. W. Liebermann and R. J. Zollweg, Electrical conductivity of nonideal plasmas, *Journal of Applied Physics*, 62 (9) (1987) 3621-3627.
- [10] K. Kim, Time-dependent one-dimensional modeling of pulsed plasma discharge in a capillary plasma device, *IEEE Transactions on Plasma Science*, 31

- (4) (2003) 729-735.
- [11] W. Jiang and K. Yatsui, Pulsed wire discharge for nanosized powder synthesis, *IEEE Transactions on Plasma Science*, 26 (5) (1998) 1498-1501.
- [12] P. V. Ananthapadmanabhan, K. P. Sreekumar, N. Venkatramani, P. K. Sinha and P. R. Taylor, Characterization of plasma-synthesized alumina, *Journal of Alloys and Compounds*, 244 (1996) 70-74.